Energy release rate of the fiber/matrix interface crack in cross-ply $[0^\circ_{2kn}, 90^\circ_n]_S$ laminates under transverse loading: debond-bimaterial interface interaction

Luca Di Stasio[a,b], Janis Varna[b], Zoubir Ayadi[a]

[a] *Université de Lorraine, EEIGM, IJL, 6 Rue Bastien Lepage, F-54010 Nancy, France*
[b] *Luleå University of Technology, University Campus, SE-97187 Luleå, Sweden*

Abstract

The effects of crack shielding, fiber content and ratio of 0° to 90° ply thickness on fiber/matrix debond growth in thin cross-ply laminates are investigated with Representative Volume Elements (RVEs) of different ordered microstructures. Debond growth is characterized by the estimation of the Energy Release Rates (ERRs) using the Virtual Crack Closure Technique (VCCT) and the J-integral. It is found that

Keywords: Polymer-matrix Composites (PMCs), Thin-ply, Transverse Failure, Debonding, Finite Element Analysis (FEA)

1. Introduction

Since the development of the *spred tow* technology or "FUKUI method" [1, 2], significant efforts have been directed toward the characterization of *thin-ply* laminates [3, 4, 5, 6, 7, 8, 9, 10, 11, 12, 13, 14, 15] and their application to mission-critical structures in the aerospace sector [16, 17, 18, 19].

2. RVE models & FE discretization

2.1. Models of Representative Volume Element(RVE)

We start by describing the different idealized micro-structures considered and the corresponding repeating element or RVE used to model them. Fig. 1,

Fig. 2 and Fig. 3

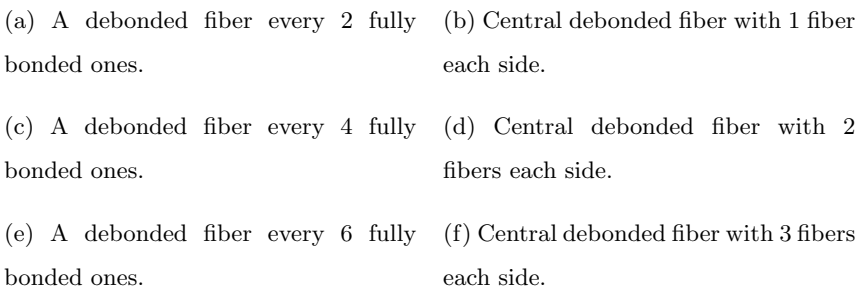

(a) A debonded fiber every 2 fully bonded ones.

(b) Central debonded fiber with 1 fiber each side.

(c) A debonded fiber every 4 fully bonded ones.

(d) Central debonded fiber with 2 fibers each side.

(e) A debonded fiber every 6 fully bonded ones.

(f) Central debonded fiber with 3 fibers each side.

Figure 1: Models of $[0_n^\circ, 90^\circ]_S$ laminates in which the central 90° ply possesses a single layer of fibers and debonds repeating at different distances (left column), and corresponding Representative Volume Elements (right column) with symmetry applied on the lower boundary line. The interface crack is represented in red.

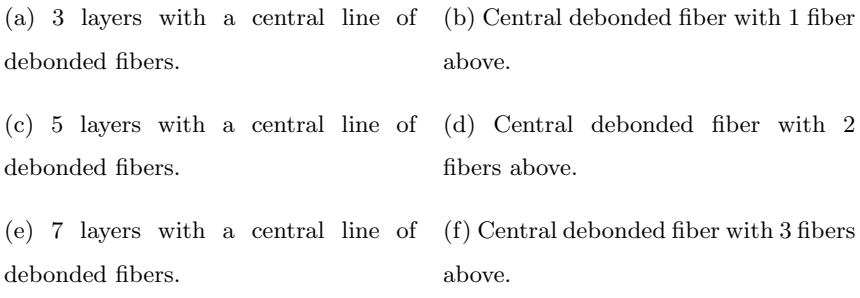

(a) 3 layers with a central line of debonded fibers.

(b) Central debonded fiber with 1 fiber above.

(c) 5 layers with a central line of debonded fibers.

(d) Central debonded fiber with 2 fibers above.

(e) 7 layers with a central line of debonded fibers.

(f) Central debonded fiber with 3 fibers above.

Figure 2: Models of $[0_n^\circ, 90^\circ]_S$ laminates in which the central 90° ply possesses a central line of debonded fibers (left column), and corresponding Representative Volume Elements (right column) with symmetry applied on the lower boundary line. The interface crack is represented in red.

2.2. Finite Element (FE) discretization

We describe the model implemented: schematic + description of parameters, formulation (LEFM, frictionless contact, VCCT, J-Integral), implementation of BCs, mesh. Fig. 5

We mention the validation of the model with respect to BEM results by referring to the other paper.

(a) 3 layers with a debonded fiber every 2 fully bonded ones in the central line of fibers.

(b) Central debonded fiber with 1 fiber on each side and 1 above.

(c) 3 layers with a debonded fiber every 4 fully bonded ones in the central line of fibers.

(d) Central debonded fiber with 2 fibers on each side and 1 above.

(e) 5 layers with a debonded fiber every 4 fully bonded ones in the central line of fibers.

(f) Central debonded fiber with 2 fibers on each side and 2 above.

(g) 3 layers with a debonded fiber every 6 fully bonded ones in the central line of fibers.

(h) Central debonded fiber with 3 fibers on each side and 1 above.

Figure 3: Models of$[0_n^\circ, 90^\circ]_S$ laminates in which the central 90° ply possesses multiple layers of fibers with debonds repeating at different distances in the central line of fibers (left column), and corresponding Representative Volume Elements (right column) with symmetry applied on the lower boundary line.

(a) Single layer of debonded fibers inside a cross-ply laminates.

(b) Element with a single debonded fiber and, on the top surface, coupled vertical displacement and linearly distributed horizontal displacement.

Figure 4: Models of $[0_n^\circ, 90^\circ]_S$ laminates in which fibers belonging to the central 90° ply are all debonded (left column), and corresponding Representative Volume Elements (right column) with symmetry applied on the lower boundary line.

(a) Schematic of the model with its main parameters.

(b) Detail of the mesh in the crack tip's neighborhood.

Figure 5: Details and main parameters of the Finite Element model.

3. Results & Discussion

3.1. Effect of Fiber Volume Fraction

The effect is similar for all the different BC cases, it's enough to show some of them to exemplify. G_I in Fig. 6, G_{II} in Fig. 7.

Graphics of ERR vs $\Delta\theta$, one curve for each V_f, one graphic for each selected BC. Selected BC: free, coupling, some examples with fibers (see captions).

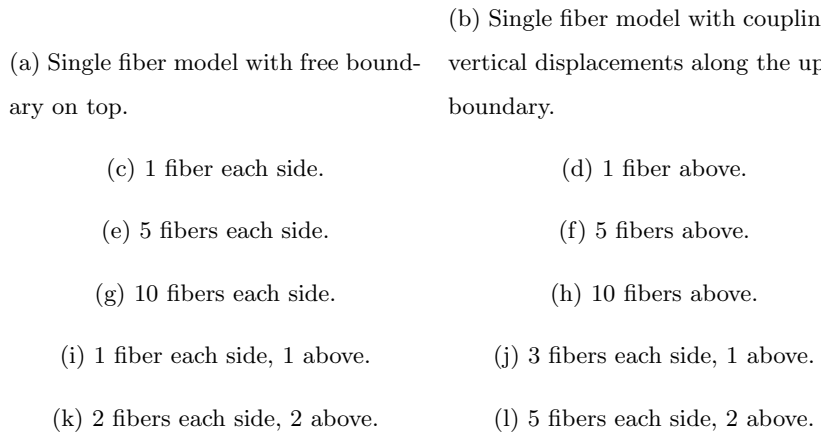

(a) Single fiber model with free boundary on top.

(b) Single fiber model with coupling of vertical displacements along the upper boundary.

(c) 1 fiber each side.

(d) 1 fiber above.

(e) 5 fibers each side.

(f) 5 fibers above.

(g) 10 fibers each side.

(h) 10 fibers above.

(i) 1 fiber each side, 1 above.

(j) 3 fibers each side, 1 above.

(k) 2 fibers each side, 2 above.

(l) 5 fibers each side, 2 above.

Figure 6: A view of the effect of fiber volume fraction on Mode I ERR across different models.

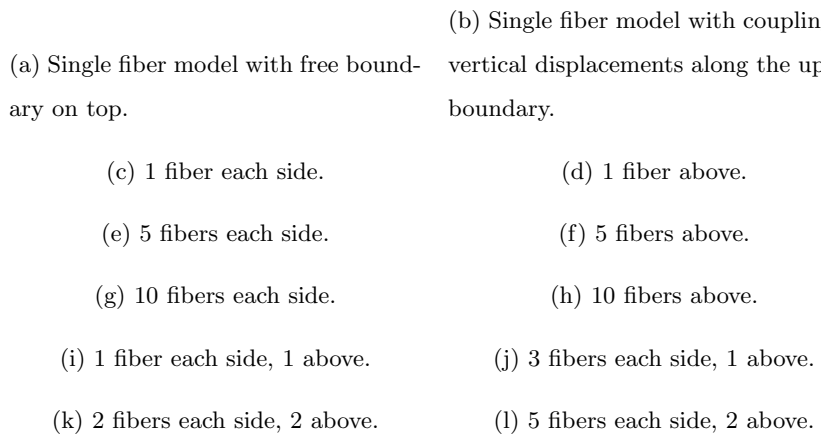

(a) Single fiber model with free boundary on top.

(b) Single fiber model with coupling of vertical displacements along the upper boundary.

(c) 1 fiber each side.

(d) 1 fiber above.

(e) 5 fibers each side.

(f) 5 fibers above.

(g) 10 fibers each side.

(h) 10 fibers above.

(i) 1 fiber each side, 1 above.

(j) 3 fibers each side, 1 above.

(k) 2 fibers each side, 2 above.

(l) 5 fibers each side, 2 above.

Figure 7: A view of the effect of fiber volume fraction on Mode II ERR across different models.

3.2. *Interaction between debonds in a* $90°$ *ply with a single layer of fibers inside a* $[0°_n, 90°]_S$ *laminate*

We start with a simpler (2 parameters: number of fibers in the horizontal directions + bounding ply thickness) but more extreme model: central $90°$ ply with one line of fibers. What's the effect on G_I and G_{II}? What's the effect of $0°$ ply's thicknesses? Reference to Kies strain magnification. G_I in Fig. 8, G_{II} in Fig. 9.

One graphic for each V_f (30%,50%,60%,65%) and thickness ratio (1, 10), one curve for each case of fibers on the side (1, 2, 3, 5, 10, 50, 100) + curve for equivalent BC ()(Fig. 8, Fig. 9). Focus is effect of debond distribution in the horizontal direction.

(a) $V_f = 30\%$, $\frac{t_{0°}}{t_{90°}} = 1.$ (b) $V_f = 30\%$, $\frac{t_{0°}}{t_{90°}} = 10.$

(c) $V_f = 50\%$, $\frac{t_{0°}}{t_{90°}} = 1.$ (d) $V_f = 50\%$, $\frac{t_{0°}}{t_{90°}} = 10.$

(e) $V_f = 60\%$, $\frac{t_{0°}}{t_{90°}} = 1.$ (f) $V_f = 60\%$, $\frac{t_{0°}}{t_{90°}} = 10.$

(g) $V_f = 65\%$, $\frac{t_{0°}}{t_{90°}} = 1.$ (h) $V_f = 65\%$, $\frac{t_{0°}}{t_{90°}} = 10.$

Figure 8: Effect of the interaction between debonds appearing at regular intervals on Mode I ERR in a $[0°_n, 90°]_S$ laminates in which the central $90°$ ply possesses a single layer of fibers at different levels of fiber volume fraction V_f.

(a) $V_f = 30\%$, $\frac{t_{0°}}{t_{90°}} = 1.$ (b) $V_f = 30\%$, $\frac{t_{0°}}{t_{90°}} = 10.$

(c) $V_f = 50\%$, $\frac{t_{0°}}{t_{90°}} = 1.$ (d) $V_f = 50\%$, $\frac{t_{0°}}{t_{90°}} = 10.$

(e) $V_f = 60\%$, $\frac{t_{0°}}{t_{90°}} = 1.$ (f) $V_f = 60\%$, $\frac{t_{0°}}{t_{90°}} = 10.$

(g) $V_f = 65\%$, $\frac{t_{0°}}{t_{90°}} = 1.$ (h) $V_f = 65\%$, $\frac{t_{0°}}{t_{90°}} = 10.$

Figure 9: Effect of the interaction between debonds appearing at regular intervals on Mode II ERR in a single-ply laminate with a single layer of fibers at different levels of fiber volume fraction V_f.

One graphic for each V_f (30%,50%,60%,65%) and selected cases of fibers on the side (1, 3, 10), one curve for thickness ratio (1, 10) + curve for corresponding UD model + curve for equivalent BC (vertical displacement coupling+linear horizontal displacement)(Fig. 10, Fig. 11). Focus is effect of thickness of bounding plies.

(a) $V_f = 30\%$, 1 fiber on each side.

(b) $V_f = 30\%$, 3 fibers on each side.

(c) $V_f = 30\%$, 10 fibers on each side.

(d) $V_f = 50\%$, 1 fiber on each side.

(e) $V_f = 50\%$, 3 fibers on each side.

(f) $V_f = 50\%$, 10 fibers on each side.

(g) $V_f = 50\%$, 1 fiber on each side.

(h) $V_f = 50\%$, 3 fibers on each side.

(i) $V_f = 50\%$, 10 fibers on each side.

(j) $V_f = 65\%$, 1 fiber on each side.

(k) $V_f = 65\%$, 3 fibers on each side.

(l) $V_f = 65\%$, 10 fibers on each side.

Figure 10: Effect of 0° ply's thickness on the interaction between debonds appearing at regular intervals on Mode I ERR in a $[0^\circ_n, 90^\circ]_S$ laminate in which the central 90° ply possesses a single layer of fibers at different levels of fiber volume fraction V_f.

3.3. Interaction between layers of fully bonded fibers and a centrally located line of debonded fibers in a 90° ply inside a $[0^\circ_n, 90^\circ]_S$ laminate

We then move to a ply with multiple lines of fibers and only debonded fibers in the central one (2 parameters: number of fibers in vertical direction + bounding ply thickness, a bit closer to real plies). G_I in Fig. 12, G_{II} in Fig. 13.

One graphic for each V_f (30%,50%,60%,65%) and thickness ratio (1, 10), one curve for each case of fibers on top (1, 2, 3, 5, 10, 50, 100) + curve for equivalent BC (Fig. 12, Fig. 13). Focus is effect of debond distribution in the vertical direction.

(a) $V_f = 30\%$, 1 fiber on each side.

(b) $V_f = 30\%$, 3 fibers on each side.

(c) $V_f = 30\%$, 10 fibers on each side.

(d) $V_f = 50\%$, 1 fiber on each side.

(e) $V_f = 50\%$, 3 fibers on each side.

(f) $V_f = 50\%$, 10 fibers on each side.

(g) $V_f = 50\%$, 1 fiber on each side.

(h) $V_f = 50\%$, 3 fibers on each side.

(i) $V_f = 50\%$, 10 fibers on each side.

(j) $V_f = 65\%$, 1 fiber on each side.

(k) $V_f = 65\%$, 3 fibers on each side.

(l) $V_f = 65\%$, 10 fibers on each side.

Figure 11: Effect of 0° ply's thickness on the interaction between debonds appearing at regular intervals on Mode II ERR in a $[0_n^\circ, 90^\circ]_S$ laminate in which the central 90° ply possesses a single layer of fibers at different levels of fiber volume fraction V_f.

(a) $V_f = 30\%$, $\frac{t_{0^\circ}}{t_{90^\circ}} = 1$.

(b) $V_f = 30\%$, $\frac{t_{0^\circ}}{t_{90^\circ}} = 10$.

(c) $V_f = 50\%$, $\frac{t_{0^\circ}}{t_{90^\circ}} = 1$.

(d) $V_f = 50\%$, $\frac{t_{0^\circ}}{t_{90^\circ}} = 10$.

(e) $V_f = 60\%$, $\frac{t_{0^\circ}}{t_{90^\circ}} = 1$.

(f) $V_f = 60\%$, $\frac{t_{0^\circ}}{t_{90^\circ}} = 10$.

(g) $V_f = 65\%$, $\frac{t_{0^\circ}}{t_{90^\circ}} = 1$.

(h) $V_f = 65\%$, $\frac{t_{0^\circ}}{t_{90^\circ}} = 10$.

Figure 12: Influence of layers of fully bonded fibers on debond's growth in Mode I ERR in a centrally located line of debonded fibers at different levels of fiber volume fraction V_f and thickness ratios.

(a) $V_f = 30\%$, $\frac{t_{0^\circ}}{t_{90^\circ}} = 1$.

(b) $V_f = 30\%$, $\frac{t_{0^\circ}}{t_{90^\circ}} = 10$.

(c) $V_f = 50\%$, $\frac{t_{0^\circ}}{t_{90^\circ}} = 1$.

(d) $V_f = 50\%$, $\frac{t_{0^\circ}}{t_{90^\circ}} = 10$.

(e) $V_f = 60\%$, $\frac{t_{0^\circ}}{t_{90^\circ}} = 1$.

(f) $V_f = 60\%$, $\frac{t_{0^\circ}}{t_{90^\circ}} = 10$.

(g) $V_f = 65\%$, $\frac{t_{0^\circ}}{t_{90^\circ}} = 1$.

(h) $V_f = 65\%$, $\frac{t_{0^\circ}}{t_{90^\circ}} = 10$.

Figure 13: Influence of layers of fully bonded fibers on debond's growth in Mode II ERR in a centrally located line of debonded fibers at different levels of fiber volume fraction V_f and thickness ratios.

One graphic for each V_f (30%,50%,60%,65%) and selected cases of fibers on top (1, 3, 10), one curve for thickness ratio (1, 10) + curve for corresponding UD model + curve for equivalent BC (vertical displacement coupling+linear horizontal displacement)(Fig. 14, Fig. 15). Focus is effect of thickness of bounding plies.

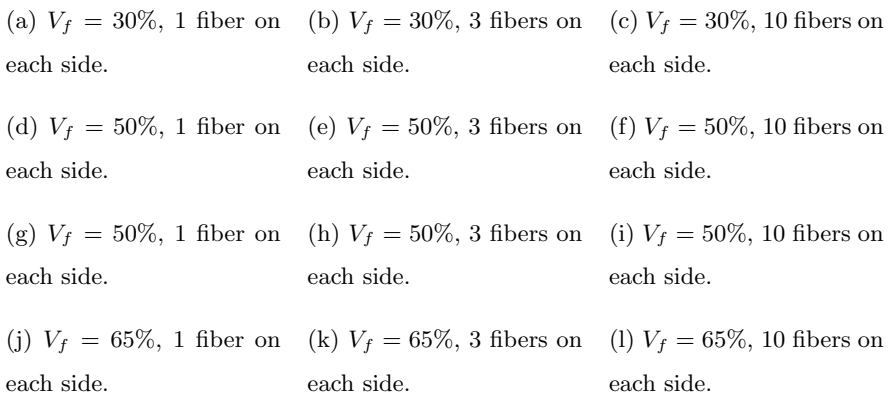

(a) $V_f = 30\%$, 1 fiber on each side. (b) $V_f = 30\%$, 3 fibers on each side. (c) $V_f = 30\%$, 10 fibers on each side.

(d) $V_f = 50\%$, 1 fiber on each side. (e) $V_f = 50\%$, 3 fibers on each side. (f) $V_f = 50\%$, 10 fibers on each side.

(g) $V_f = 50\%$, 1 fiber on each side. (h) $V_f = 50\%$, 3 fibers on each side. (i) $V_f = 50\%$, 10 fibers on each side.

(j) $V_f = 65\%$, 1 fiber on each side. (k) $V_f = 65\%$, 3 fibers on each side. (l) $V_f = 65\%$, 10 fibers on each side.

Figure 14: Effect of 0° ply's thickness on the influence of layers of fully bonded fibers on debond's growth in Mode I ERR in a centrally located line of debonded fibers in the central 90° ply of a $[0^\circ_n, 90^\circ]_S$ laminate at different levels of fiber volume fraction V_f.

3.4. Interaction of debonds within a 90° ply with multiple layers of fibers inside a $[0^\circ_n, 90^\circ]_S$ laminate

Finally models that are closer to real laminates and are more complex (3 parameters: number of fibers along the horizontal direction + number of layers in the vertical one + bounding ply thickness). G_I in Fig. 16, G_{II} in Fig. 17.

One graphic for each V_f (30%,50%,60%,65%) and thickness ratio (1, 10), one curve for each selected case of fibers on side and on top ([n. on side, n. on top]: [1,1], [2,1], [2,2], [5,1], [5,5], [10,1], [10,10]) + curve for equivalent BC (Fig. 12, Fig. 17). Focus is effect of debond distribution in the horizontal and vertical direction.

(a) $V_f = 30\%$, 1 fiber on each side.

(b) $V_f = 30\%$, 3 fibers on each side.

(c) $V_f = 30\%$, 10 fibers on each side.

(d) $V_f = 50\%$, 1 fiber on each side.

(e) $V_f = 50\%$, 3 fibers on each side.

(f) $V_f = 50\%$, 10 fibers on each side.

(g) $V_f = 50\%$, 1 fiber on each side.

(h) $V_f = 50\%$, 3 fibers on each side.

(i) $V_f = 50\%$, 10 fibers on each side.

(j) $V_f = 65\%$, 1 fiber on each side.

(k) $V_f = 65\%$, 3 fibers on each side.

(l) $V_f = 65\%$, 10 fibers on each side.

Figure 15: Effect of 0° ply's thickness on the influence of layers of fully bonded fibers on debond's growth in Mode I ERR in a centrally located line of debonded fibers in the central 90° ply of a $[0^\circ_n, 90^\circ]_S$ laminate at different levels of fiber volume fraction V_f.

(a) $V_f = 30\%$, $\frac{t_{0^\circ}}{t_{90^\circ}} = 1$.

(b) $V_f = 30\%$, $\frac{t_{0^\circ}}{t_{90^\circ}} = 10$.

(c) $V_f = 50\%$, $\frac{t_{0^\circ}}{t_{90^\circ}} = 1$.

(d) $V_f = 50\%$, $\frac{t_{0^\circ}}{t_{90^\circ}} = 10$.

(e) $V_f = 60\%$, $\frac{t_{0^\circ}}{t_{90^\circ}} = 1$.

(f) $V_f = 60\%$, $\frac{t_{0^\circ}}{t_{90^\circ}} = 10$.

(g) $V_f = 65\%$, $\frac{t_{0^\circ}}{t_{90^\circ}} = 1$.

(h) $V_f = 65\%$, $\frac{t_{0^\circ}}{t_{90^\circ}} = 10$.

Figure 16: Effect of the interaction of debonds within a 90° ply with multiple layers of fibers on debond's growth in Mode I ERR at different levels of fiber volume fraction V_f and thickness ratios.

(a) $V_f = 30\%$, $\frac{t_{0^\circ}}{t_{90^\circ}} = 1$.

(b) $V_f = 30\%$, $\frac{t_{0^\circ}}{t_{90^\circ}} = 10$.

(c) $V_f = 50\%$, $\frac{t_{0^\circ}}{t_{90^\circ}} = 1$.

(d) $V_f = 50\%$, $\frac{t_{0^\circ}}{t_{90^\circ}} = 10$.

(e) $V_f = 60\%$, $\frac{t_{0^\circ}}{t_{90^\circ}} = 1$.

(f) $V_f = 60\%$, $\frac{t_{0^\circ}}{t_{90^\circ}} = 10$.

(g) $V_f = 65\%$, $\frac{t_{0^\circ}}{t_{90^\circ}} = 1$.

(h) $V_f = 65\%$, $\frac{t_{0^\circ}}{t_{90^\circ}} = 10$.

Figure 17: Effect of the interaction of debonds within a 90° ply with multiple layers of fibers on debond's growth in Mode II ERR at different levels of fiber volume fraction V_f and thickness ratios.

One graphic for each V_f (30%,50%,60%,65%) and selected cases of fibers on side and on top ([1,1], [5,1], [5,5]), one curve for thickness ratio (1, 10) + curve for corresponding UD model + curve for equivalent BC (vertical displacement coupling+linear horizontal displacement)(Fig. 18, Fig. 19). Focus is effect of thickness of bounding plies.

(a) $V_f = 30\%$, 1 fiber on each side.	(b) $V_f = 30\%$, 3 fibers on each side.	(c) $V_f = 30\%$, 10 fibers on each side.
(d) $V_f = 50\%$, 1 fiber on each side.	(e) $V_f = 50\%$, 3 fibers on each side.	(f) $V_f = 50\%$, 10 fibers on each side.
(g) $V_f = 50\%$, 1 fiber on each side.	(h) $V_f = 50\%$, 3 fibers on each side.	(i) $V_f = 50\%$, 10 fibers on each side.
(j) $V_f = 65\%$, 1 fiber on each side.	(k) $V_f = 65\%$, 3 fibers on each side.	(l) $V_f = 65\%$, 10 fibers on each side.

Figure 18: Effect of 0° ply's thickness on debond's growth in Mode I ERR within the 90° ply with multiple layers of fibers of a $[0^\circ_n, 90^\circ]_S$ laminate at different levels of fiber volume fraction V_f.

4. Conclusions & Outlook

Acknowledgements

Luca Di Stasio gratefully acknowledges the support of the European School of Materials (EUSMAT) through the DocMASE Doctoral Programme and the European Commission through the Erasmus Mundus Programme.

References

[1] K. Kawabe, New spreading technology for carbon fiber tow and its application to composite materials, Sen'i Gakkaishi 64 (8) (2008) 262–267.

(a) $V_f = 30\%$, 1 fiber on each side.

(b) $V_f = 30\%$, 3 fibers on each side.

(c) $V_f = 30\%$, 10 fibers on each side.

(d) $V_f = 50\%$, 1 fiber on each side.

(e) $V_f = 50\%$, 3 fibers on each side.

(f) $V_f = 50\%$, 10 fibers on each side.

(g) $V_f = 50\%$, 1 fiber on each side.

(h) $V_f = 50\%$, 3 fibers on each side.

(i) $V_f = 50\%$, 10 fibers on each side.

(j) $V_f = 65\%$, 1 fiber on each side.

(k) $V_f = 65\%$, 3 fibers on each side.

(l) $V_f = 65\%$, 10 fibers on each side.

Figure 19: Effect of 0° ply's thickness on debond's growth in Mode II ERR within the 90° ply with multiple layers of fibers of a $[0_n^\circ, 90^\circ]_S$ laminate at different levels of fiber volume fraction V_f.

doi:10.2115/fiber.64.p_262.
URL https://doi.org/10.2115/fiber.64.p_262

[2] K. Kawabe, H. Sasayama, S. Tomoda, New carbon fiber tow-spread technology and applications to advanced composite materials, SAMPE Journal 45 (2) (2008) 6–17.
URL https://researchmap.jp/?action=cv_download_main&upload_id=161885

[3] H. Sasayama, K. Kawabe, S. Tomoda, I. Ohsawa, K. Kageyama, N. Ogata, Effect of lamina thickness on first ply failure in multidirectionally laminated composites, in: Proceedings of the 8^{th} Japan SAMPE Symposium, SAMPE, 2003.

[4] K. Yamaguchi, H. Hahn, The improved ply cracking resistance of thin-ply laminates, in: Proceedings of the 15^{th} International Conference on Composite Materials (ICCM-15), SAMPE, 2005.

[5] S. Tsai, S. Sihn, R. Kim, Thin ply composites, in: Proceedings of 46^{th}

AIAA/ASME/AHS/ASC Structures, Structural Dynamics & Materials Conference, 2005.

[6] S. Sihn, R. Kim, K. Kawabe, S. Tsai, Experimental studies of thin-ply laminated composites, Composites Science and Technology 67 (6) (2007) 996–1008. doi:10.1016/j.compscitech.2006.06.008.
URL https://doi.org/10.1016/j.compscitech.2006.06.008

[7] T. Yokozeki, Y. Aoki, T. Ogasawara, Experimental characterization of strength and damage resistance properties of thin-ply carbon fiber/toughened epoxy laminates, Composite Structures 82 (3) (2008) 382–389. doi:10.1016/j.compstruct.2007.01.015.
URL https://doi.org/10.1016/j.compstruct.2007.01.015

[8] T. Yokozeki, A. Kuroda, A. Yoshimura, T. Ogasawara, T. Aoki, Damage characterization in thin-ply composite laminates under out-of-plane transverse loadings, Composite Structures 93 (1) (2010) 49–57. doi:10.1016/j.compstruct.2010.06.016.
URL https://doi.org/10.1016/j.compstruct.2010.06.016

[9] H. Saito, H. Takeuchi, I. Kimpara, Experimental evaluation of the damage growth restraining in 90 layer of thin-ply cfrp cross-ply laminates, Advanced Composite Materials 21 (1) (2012) 57–66. doi:10.1163/156855112X629522.

[10] A. Arteiro, G. Catalanotti, J. Xavier, P. Camanho, Notched response of non-crimp fabric thin-ply laminates, Composites Science and Technology 79 (2013) 97–114. doi:10.1016/j.compscitech.2013.02.001.
URL https://doi.org/10.1016/j.compscitech.2013.02.001

[11] A. Arteiro, G. Catalanotti, J. Xavier, P. Camanho, Large damage capability of non-crimp fabric thin-ply laminates, Composites Part A: Applied Science and Manufacturing 63 (2014) 110–122. doi:10.1016/j.compositesa.

2014.04.002.
URL https://doi.org/10.1016/j.compositesa.2014.04.002

[12] R. Amacher, J. Cugnoni, J. Botsis, L. Sorensen, W. Smith, C. Dransfeld, Thin ply composites: Experimental characterization and modeling of size-effects, Composites Science and Technology 101 (2014) 121–132. doi:10.1016/j.compscitech.2014.06.027.
URL https://doi.org/10.1016/j.compscitech.2014.06.027

[13] G. Guillamet, A. Turon, J. Costa, J. Renart, P. Linde, J. Mayugo, Damage occurrence at edges of non-crimp-fabric thin-ply laminates under off-axis uniaxial loading, Composites Science and Technology 98 (2014) 44–50. doi:10.1016/j.compscitech.2014.04.014.
URL https://doi.org/10.1016/j.compscitech.2014.04.014

[14] C. Huang, S. Ju, M. He, Q. Zheng, Y. He, J. Xiao, J. Zhang, D. Jiang, Identification of failure modes of composite thin-ply laminates containing circular hole under tension by acoustic emission signals, Composite Structures 206 (2018) 70–79. doi:10.1016/j.compstruct.2018.08.019.
URL https://doi.org/10.1016/j.compstruct.2018.08.019

[15] J. Cugnoni, R. Amacher, S. Kohler, J. Brunner, E. Kramer, C. Dransfeld, W. Smith, K. Scobbie, L. Sorensen, J. Botsis, Towards aerospace grade thin-ply composites: Effect of ply thickness, fibre, matrix and interlayer toughening on strength and damage tolerance, Composites Science and Technology 168 (2018) 467–477. doi:10.1016/j.compscitech.2018.08.037.
URL https://doi.org/10.1016/j.compscitech.2018.08.037

[16] J.-B. Moon, M.-G. Kim, C.-G. Kim, S. Bhowmik, Improvement of tensile properties of CFRP composites under LEO space environment by applying MWNTs and thin-ply, Composites Part A: Applied Science and Manufacturing 42 (6) (2011) 694–701. doi:10.1016/j.compositesa.2011.02.011.
URL https://doi.org/10.1016/j.compositesa.2011.02.011

[17] Y. H. N. Kim, S. Ko, W.-S. Lay, J. Tian, P. Chang, S. U. Thielk, H.-J. Bang, J. Yang, Effects of shallow biangle, thin-ply laminates on structural performance of composite wings, AIAA Journal 55 (6) (2017) 2086–2092. doi:10.2514/1.j055465.
URL https://doi.org/10.2514/1.j055465

[18] A. Kopp, S. Stappert, D. Mattsson, K. Olofsson, E. Marklund, G. Kurth, E. Mooij, E. Roorda, The aurora space launcher concept, CEAS Space Journal 10 (2) (2017) 167–187. doi:10.1007/s12567-017-0184-2.
URL https://doi.org/10.1007/s12567-017-0184-2

[19] D. A. McCarville, J. C. Guzman, A. K. Dillon, J. R. Jackson, J. O. Birkland, 3.5 Design, Manufacture and Test of Cryotank Components, Elsevier, 2018, pp. 153–179. doi:10.1016/b978-0-12-803581-8.09958-6.
URL https://doi.org/10.1016/b978-0-12-803581-8.09958-6